Am J Physiol Cell Physiol 287: C643–C654, 2004.
First published June 2, 2004; 10.1152/ajpcell.00070.2004.

Cytoskeletal mechanics in adherent human airway smooth muscle cells: probe specificity and scaling of protein-protein dynamics

Marina Puig-de-Morales,[1] Emil Millet,[1] Ben Fabry,[2] Daniel Navajas,[3] Ning Wang,[1] James P. Butler,[1] and Jeffrey J. Fredberg[1]

[1]*Physiology Program, Harvard School of Public Health, Boston, Massachusetts 02115;* [2]*Physics Department, Erlangen University, 91054 Erlangen, Germany; and* [3]*Unitat de Biofísica i Bioenginyeria, Facultat de Medicina, Universitat de Barcelona-IDIBAPS, Barcelona 08036, Spain*

Submitted 5 February 2004; accepted in final form 5 May 2004

Puig-de-Morales, Marina, Emil Millet, Ben Fabry, Daniel Navajas, Ning Wang, James P. Butler, and Jeffrey J. Fredberg. Cytoskeletal mechanics in adherent human airway smooth muscle cells: probe specificity and scaling of protein-protein dynamics. *Am J Physiol Cell Physiol* 287: C643–C654, 2004. First published June 2, 2004; 10.1152/ajpcell.00070.2004.—We probed elastic and loss moduli in the adherent human airway smooth muscle cell through a variety of receptor systems, each serving as a different molecular window on cytoskeletal dynamics. Coated magnetic microbeads were attached to the cell surface via coating-receptor binding. A panel of bead coatings was investigated: a peptide containing the sequence RGD, vitronectin, urokinase, activating antibody against β_1-integrin, nonactivating antibody against β_1-integrin, blocking antibody against β_1-integrin, antibody against β_1-integrin, and acetylated low-density lipoprotein. An oscillatory mechanical torque was applied to the bead, and resulting lateral displacements were measured at baseline, after actin disruption by cytochalasin D, or after contractile activation by histamine. As expected, mechanical moduli depended strongly on bead type and bead coating, differing at the extremes by as much as two orders of magnitude. In every case, however, elastic and loss moduli increased with frequency f as a weak power law, f^{x-1}. Moreover, with few exceptions, data could be scaled such that elastic and frictional responses depended solely on the power law exponent x. Taken together, these data suggest that power law behavior represents a generic feature of underlying protein-protein dynamics.

actin; cytoskeleton; magnetic twisting cytometry; scale free; viscoelasticity

MECHANICAL PROPERTIES of the cytoskeleton govern the rate at which the cell can crawl, deform and remodel, and come into play in signaling responses to applied mechanical forces. Fabry et al. (19, 20) measured stiffness (elastic) and frictional (loss) moduli of adherent human airway smooth muscle (HASM) cells. They showed that with increasing frequency f of the imposed oscillatory deformation, these moduli increased as a weak power law, f^{x-1}, where the parameter x fell in the range 1.1–1.4. This power law behavior persisted over a wide frequency range (10^{-2}–10^3 Hz), applied to a variety of cell types (airway smooth muscle cells, neutrophils, pulmonary macrophages, bronchial epithelial cells, and embryonic carcinoma cells), and prevailed under a variety of interventions (contractile and relaxing agonists, and actin disrupting agents).

In those studies, it was noted that elastic moduli measured after the different manipulations defined a family of curves, all of which, when extrapolated, appeared to cross in the vicinity of a common intersection, or fixed point, at high frequency. Moreover, Fabry et al. (19, 20) showed that data for all frequencies, all cell types, and all interventions that they studied, when suitably normalized, could be collapsed onto two master relationships, one describing elasticity and the other friction, in which the power law exponent x was the central controlling parameter.

Although the collapse of diverse data is remarkable and has broad implications, in every instance Fabry's measurements probed elastic and loss moduli of the cell by using microbeads coated with the very same ligand: a peptide containing the sequence RGD (Arg-Gly-Asp). RGD-coated beads bind to the cell surface via integrins (69, 77), mostly $\alpha_5\beta_1$, which cluster in localized attachment domains and assemble into adhesion complexes (56, 74, 84, 90). Consequently, this process inevitably alters cellular mechanical responses (8, 12, 43, 44, 61, 84). It is possible, therefore, that the power law behavior reported by Fabry et al. (19, 20), as well as the collapse of all data onto master relationships, might reflect nothing more than the particular ligand-receptor complex through which the cell was probed. If so, then Fabry's results would not be generalizable. In the present study, we used a wide panel of bead coatings to examine that possibility.

MATERIALS AND METHODS

Microbead coating protocols. We used two types of coatings: ligands (nonantibodies) and antibodies. For the ligand group we used ferrimagnetic microbeads (solid Fe_3O_4, 4.5-μm diameter) produced in our laboratory (18). For the antibody group we used polystyrene ferromagnetic microbeads (containing CrO_2, 4.5-μm diameter) precoated with goat anti-mouse Fc groups, through which the antibody Fc domain attached to the bead surface, leaving the active site (Fab) available for binding to cell surface receptors.

For the ligand group, beads were coated with one of the following: a peptide containing the sequence RGD, vitronectin (VN), urokinase plasminogen activator (uPA), or acetylated low-density lipoprotein (AcLDL). Because each of these ligands binds to the cell in a different way (31), the coupling of the bead to the cytoskeleton (CSK) depends on the bead coating (Fig. 1). RGD peptide binds primarily to β_1-integrin. VN is also an RGD site-dependent adhesive glycoprotein and binds mainly to β_3-integrin (83); both VN and RGD bind to the underlying CSK with the assembly of focal contacts. uPA binds to the uPA receptor, which in turn binds to integrins through caveolin and mediates mechanical force transmission to the CSK by indirect attachment (9, 65, 66, 87). AcLDL binds to LDL receptor, a nonad-

Address for reprint requests and other correspondence: M. Puig-de-Morales, Physiology Program, Harvard School of Public Health, 665 Huntington Ave., Boston, MA 02115 (E-mail: mpuigdem@hsph.harvard.edu).

The costs of publication of this article were defrayed in part by the payment of page charges. The article must therefore be hereby marked "*advertisement*" in accordance with 18 U.S.C. Section 1734 solely to indicate this fact.

 0363-6143/04 $5.00 Copyright © 2004 the American Physiological Society

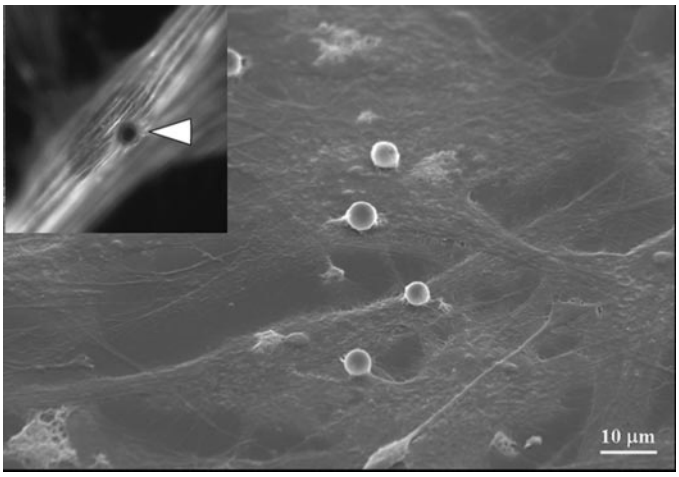

Fig. 1. Electron micrograph showing microbeads (4.5 μm) attached to the surface of human airway smooth muscle (HASM) cells. Beads oscillate back and forth in response to a sinusoidal magnetic field. The deformation is transmitted from the bead through the coating-receptor complex to the cell body. Because of its elasticity and friction, the cell opposes bead motion. From the applied torque and the resulting bead displacement, we compute the stiffness and the dissipative properties of the cell. *Inset*: immunofluorescent image of a HASM cell stained for F-actin. Arrowhead shows an RGD-coated bead bound tightly to the underlying actin cytoskeleton.

hesion scavenger receptor that does not bind to the CSK (36, 69, 70, 84). Each ligand was bound onto the bead surface (50 μg ligand/mg beads) by overnight incubation at 4°C in carbonate buffer (pH 9.4).

For the antibody group, beads were coated with different mouse anti-human anti-β_1- and anti-β_3-integrins: an activating antibody against β_1-integrin (MAB2000), a nonactivating antibody against β_1-integrin (K20), a blocking antibody against β_1-integrin (MAB1987), or an antibody against $\alpha_v\beta_3$, the main VN receptor. The activating antibody against β_1-integrin serves as a mediator of both integrin occupancy and aggregation. However, the nonactivating and blocking antibodies do not; it has been shown (12, 55, 59, 62, 63) that they do not significantly cluster F-actin, talin, α-actinin, vinculin, paxillin, or filamin. All antibodies were bound onto the bead surface (50 μg antibody/mg beads) by 30-min incubation at 4°C in phosphate-buffered saline. Finally, to estimate the influence of bead type, we studied solid Fe_3O_4 ferrimagnetic vs. polystyrene CrO_2 ferromagnetic microbeads with the same coating. We coated the polystyrene beads using the same RGD peptide as for the first group; these beads are commercially precoated with reactive carboxyl groups to which RGD peptides become attached. In each case, beads were washed and resuspended in serum-free medium supplemented with 1% BSA before the experiments.

Cell culture. Human tracheas were obtained from lung transplant donors, in accordance with procedures approved by the University of Pennsylvania Committee on Studies Involving Human Beings. Tracheal smooth muscle cells were harvested as previously described (50, 56, 67). The cells were plated in plastic flasks and maintained in nutrient mixture (Ham's) F-12 medium supplemented with 10% FCS, 100 U/ml penicillin, 100 μg/ml streptomycin, 200 μg/ml amphotericin B, 12 mM NaOH, 1.7 μM $CaCl_2$, 2 mM L-glutamine, and 25 mM HEPES. The confluent cells were serum-deprived and supplemented with 5.7 μg/ml insulin and 5 μg/ml human transferrin for 48 h before the experiment. The cells were used in *passages 4–7*.

Cell-bead preparation. Cells were trypsinized (0.25% trypsin and 1 mM EDTA), plated at confluence overnight (2×10^4 cells/well) on collagen-coated (500 ng/well) plastic wells (6.4-mm, 96-well Removawells, Immulon II; Dynatech, Chantilly, VA). In the case of beads coated with uPA, however, we used 1×10^4 cells/well grown to subconfluence; this was necessary because beads coated with uPA do not bind to confluent cells (68).

Cells were washed twice with serum-free medium supplemented with 1% BSA, coated beads were then added for 15–20 min at 37°C to allow for the binding to the receptors on the cell surface, and wells were washed twice with serum-free medium supplemented with 1% BSA to remove any unbound beads The final concentration was approximately 1 bead/cell. Finally, measurements were performed as described below.

Experiments for each bead type and each bead coating were done on five separate experimental days and measured in 15–30 cell wells for each condition. These wells were further distributed among three conditions: cells not treated (baseline); cells treated with cytochalasin D (2×10^{-6} M), an actin network disruptor, for 15 min; and cells treated with histamine (10^{-4} M), a contractile agonist, for 15 min.

In a separate series of experiments, we established the specificity of bead binding. Cells were pretreated for 30 min with the corresponding soluble coating material in the media as a competitor (0, 5, and 50 mg/ml), and the number of beads that subsequently bound was measured with and without the competitor. All coating showed specificity. We also measured cell stiffness as a function of the concentration of bead coating material in which the beads were incubated (as described above). For each bead coating we found that measured stiffness increased with concentration but eventually saturated at high concentration. Similarly, we measured the number of beads bound to each cell as a function of the concentration of bead coating material in which the beads were incubated, and the number of attached beads increased with concentration but eventually saturated at high concentrations. All data reported were obtained with the use of saturating concentrations.

Magnetic twisting cytometry with optical detection. The experimental setup is described elsewhere (19, 20). Briefly, wells containing cells with beads attached were placed on an inverted microscope. Beads were magnetized horizontally and then subjected to a vertical oscillatory field. This oscillatory field causes a mechanical torque that twists the bead toward alignment with the direction of the imposed field. This torque is transmitted from the bead through the ligand-receptor complex to the cell body, which, because of its elasticity and friction, impedes the bead motion. Measurements were performed at oscillatory frequencies between 10^{-1} and 10^3 Hz, and the amplitude of the oscillatory magnetic field was first adjusted to keep the mean bead displacement within the linear range for each of the three conditions with each different coating and was then kept at the same magnetic amplitude across frequencies; data from beads with amplitude >500 nm were discarded. Oscillatory lateral displacements of each bead were recorded using a charge-coupled device camera with an exposure time of 0.1 ms. Bead position was determined using an intensity-weighted center-of-mass algorithm yielding accuracy in the bead position better than 5 nm.

The complex elastic modulus was defined at each radian frequency, ω, as $g^*(\omega) = T^*/d^*$, where T* and d* are the Fourier coefficients of the oscillatory specific torque and displacement, $\omega = 2\pi f$, and the specific torque is the torque per unit bead volume. This is equivalent to computing the components of bead displacement both in phase and out of phase with the applied specific torque. As defined here, this modulus has units of pascals per nanometer. Such measurements can be transformed into traditional elastic and loss moduli (in units of Pa) through multiplication by a geometric scale factor, α, which depends on the shape and thickness of the cell and the degree of the bead embedding. Finite element analysis of cell deformation sets α at roughly 6.8 μm (60), assuming homogeneous and isotropic elastic properties with 10% of the bead diameter embedded in a cell 5 μm high.

Statistical evaluation of power law behavior. For a material whose stress relaxation function is At^{1-x}, the complex modulus is given by the power law,

$$g^*(\omega) = (i\omega)^{x-1}A\Gamma(2-x) + i\mu\omega, \quad (1)$$

where $i\mu\omega$ corresponds to small, additive Newtonian viscosity taken to be mechanically in parallel, A is a scale factor, $x - 1$ is the power law exponent, $\Gamma(\cdot)$ is the gamma function, and $i^2 = -1$. *Equation 1* is called the structural damping law (20, 27, 28). We measured the complex elastic modulus $g^* = g' + ig''$, where g' and g'' are the storage and loss moduli, respectively, for each bead-cell system, and we fitted *Eq. 1* to these measurements.

In the limit that x approaches unity, the real part of g* reduces to a perfect elastic Hookean stiffness, and the imaginary part is the simple additive viscous term (20). In the limit that x approaches 2, the real part of g* vanishes, and the imaginary part corresponds to a perfect Newtonian viscous fluid of viscosity $A + \mu$. As such, x describes the transition from solidlike elastic states to fluidlike viscous states.

The variability in g* across the bead population increases with its magnitude and is approximately log normal (19). We therefore modeled the variability in g* as being proportionate; this is equivalent to having an approximately uniform (complex) variability that is additive in ln(g*). Consequently, we used the logarithm of the measured complex modulus for the individual fits to the logarithm of *Eq. 1* and for subsequent statistical analysis. In that connection, we used least-squares minimization to evaluate the parameters, and all sums of squared residuals were thus performed using logarithms of data and of prediction (20).

Existence of a fixed point. We assessed *Eq. 1* using three statistical models. In *model I*, all parameters (x_n, A_n, and μ_n) for any given coating were free to vary among the n experimental conditions ($n = 3$: baseline, histamine, cytochalasin D). In *model II*, A_n was given by $g_0/\Phi_0^{x_n-1}$, where only x_n was free to vary, implying a convergence of the curves for all three conditions in the vicinity of the coordinates (g_0, Φ_0). In *model III*, A_n and μ_n were free to vary, but the exponent x was constrained to be common over the experimental conditions, implying a parallel shift (log g* vs. log f) with treatment. *Model I* vs. *II* and *model I* vs. *III* were then compared by reduction-of-variance F-test. If the observed P value of the pairwise comparison was <0.05, we concluded that there were significant differences between models, implying that the fit of the model with fewer parameters (e.g., *model II* or *III*) was not as good as the fit using *model I*. *Models II* and *III* were not compared, because neither model is a subset of the other. Finally, for *model II*, we evaluated 95% confidence regions of g_0 and Φ_0. Software used for these procedures was the R statistical program (version 1.6.2).

Chemicals. Ham's F-12 culture medium, FCS, insulin, human transferrin, penicillin-streptomycin solution, L-glutamine, NaOH, $CaCl_2$, histamine, cytochalasin D, and BSA were obtained from Sigma Chemicals (St. Louis, MO). Fungizone and 0.02% trypsin were purchased from GIBCO (Gaithersburg, MD). Phosphate-buffered saline was obtained from BioWhittaker (Walkersville, MD). Type I rat tail collagen was purchased from Upstate Biotechnology (Lake Placid, NY). Synthetic RGD-containing peptide (Arg-Gly-Asp; Peptide 2000) was purchased from Telios Pharmaceuticals (San Diego, CA). AcLDL was purchased from Biomedical Technologies (Stoughton, MA). Human urokinase was obtained from American Diagnostica (Greenwich, CT). Human monoclonal antibodies against β_1-integrin (clones MAB1987 and MAB 2000) and against $\alpha_v\beta_3$-integrin were purchased from Chemicon (Temecula, CA). Monoclonal antibody against β_1-integrin (clone K20) was purchased from Beckman-Coulter (France). Polystyrene beads (4.5-μm diameter) with a CrO_2 surface layer, precoated with goat anti-mouse IgG for the antibody studies or precoated with reactive carboxyl groups for a separate RGD control, were purchased from Spherotech (Libertyville, IL).

RESULTS

Frequency dependence. When beads were coated with the peptide sequence containing RGD, the stiffness g' of cells in baseline conditions increased as a power law with frequency throughout the measurement range (Fig. 2*A*, circles). However, these power law relationships were quite weak. The loss modulus g'' also approximated a power law with the same exponent at low frequencies but showed stronger frequency

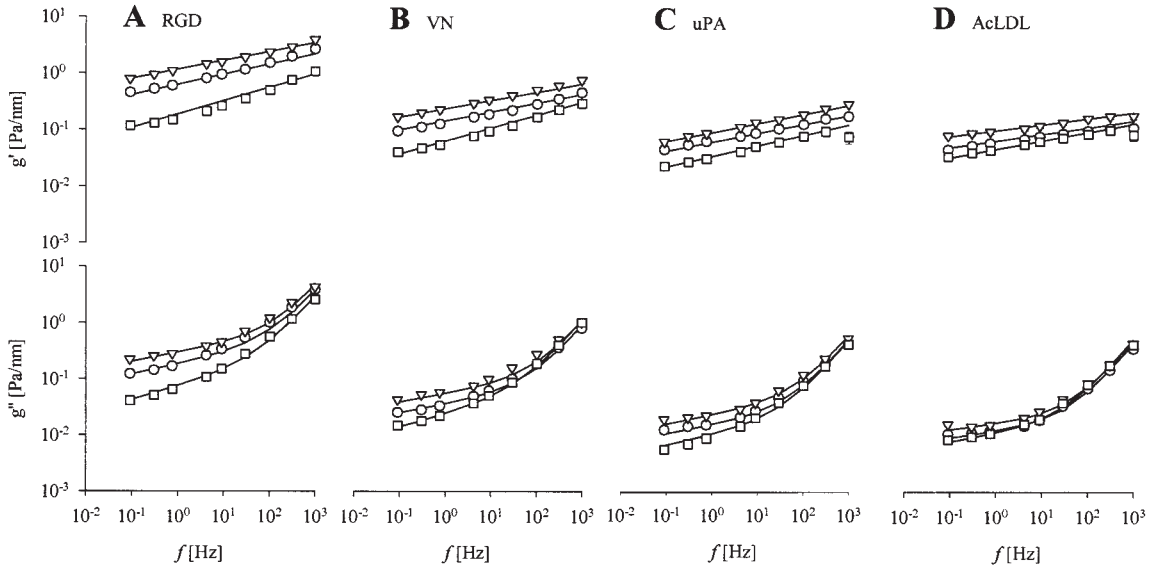

Fig. 2. Median storage modulus (g'; *top*) and loss modulus (g''; *bottom*) vs. frequency (f) for ferrimagnetic microbeads ligand coated with RGD (*A*), vitronectin (VN; *B*), urokinase plasminogen activator (uPA; *C*), and acetylated low-density lipoprotein (AcLDL; *D*) in baseline conditions (○), histamine (10^{-4} M, 15 min; ▽), and cytochalasin D (2×10^{-6} M, 15 min; □). Solid lines are fits of *Eq. 1* to median data, and error bars represent 1 SE. Variability is quantified in Table 1.

dependence at higher frequencies. When the actin network was disrupted by cytochalasin D (2×10^{-6} M), both g′ and g″ fell dramatically, and their dependence on frequency increased (Fig. 2*A*, squares). When the cells were activated by the contractile agonist histamine (10^{-4} M), g′ and g″ increased and their dependence on frequency decreased (Fig. 2*A*, triangles). All data were well described by *Eq. 1* (fits denoted by solid lines, Fig. 2*A*) and were consistent with data reported previously (16, 19, 20). Bead-by-bead variability is quantified in Table 1.

When the cell was probed with beads coated with other ligands, responses were remarkably different in magnitude but power law responses prevailed in every instance (Figs. 2 and 3). Within a given bead type but with different ligand coatings, differences in stiffness approached an order of magnitude (e.g., RGD vs. AcLDL, Fig. 2). Increases of stiffness induced by histamine and decreases of stiffness induced by cytochalasin D were evident with each of the bead coatings, but the magnitude of the induced changes was substantially attenuated when the cell was probed with beads coated with AcLDL compared with those coated with RGD; VN-coated beads were intermediate in that regard. Differences among the antibody-coated beads were smaller but appreciable. The Newtonian term μ varied little with the cellular manipulation and did so without a systemic pattern across conditions for each bead coating (Table 1).

Table 1. *Stiffness, slope, viscosity, and number of beads at baseline, histamine and cytochalasin D*

	A, Pa/nm	*x*	μ, $\times 10^{-5}$ Pa·s·nm^{-1}	*N*
RGD				
Baseline	0.41 (0.03)	1.181 (0.002)	8.8 (0.03)	1,010
Histamine	0.80 (0.05)	1.158 (0.003)	9.5 (0.05)	271
Cyt-D	0.11 (0.04)	1.238 (0.004)	6.5 (0.04)	357
VN				
Baseline	0.10 (0.04)	1.157 (0.002)	1.9 (0.03)	748
Histamine	0.17 (0.07)	1.147 (0.003)	2.4 (0.06)	228
Cyt-D	0.04 (0.06)	1.229 (0.005)	2.6 (0.06)	216
uPA				
Baseline	0.04 (0.03)	1.158 (0.002)	1.1 (0.02)	879
Histamine	0.06 (0.05)	1.161 (0.003)	1.3 (0.04)	307
Cyt-D	0.02 (0.07)	1.186 (0.006)	1.1 (0.05)	138
AcLDL				
Baseline	0.05 (0.03)	1.118 (0.002)	0.9 (0.02)	850
Histamine	0.08 (0.05)	1.105 (0.003)	1.1 (0.04)	297
Cyt-D	0.03 (0.07)	1.149 (0.006)	1.1 (0.05)	147
Anti-β_1 activating				
Baseline	0.07 (0.04)	1.134 (0.002)	2.1 (0.02)	1,003
Histamine	0.11 (0.07)	1.117 (0.003)	1.6 (0.05)	236
Cyt-D	0.03 (0.08)	1.179 (0.006)	2.0 (0.04)	157
Anti-β_1 nonactivating				
Baseline	0.04 (0.05)	1.124 (0.002)	1.6 (0.03)	523
Histamine	0.08 (0.13)	1.101 (0.005)	1.9 (0.08)	100
Cyt-D	0.04 (0.10)	1.148 (0.007)	2.0 (0.06)	126
Anti-β_1 blocking				
Baseline	0.05 (0.05)	1.132 (0.003)	1.8 (0.03)	548
Histamine	0.08 (0.12)	1.101 (0.004)	1.8 (0.08)	113
Cyt-D	0.03 (0.11)	1.160 (0.008)	1.6 (0.06)	122
Anti-$\alpha_v\beta_3$				
Baseline	0.02 (0.07)	1.127 (0.004)	1.2 (0.05)	184
Histamine	0.03 (0.13)	1.122 (0.006)	1.3 (0.07)	61
Cyt-D	0.01 (0.15)	1.157 (0.01)	1.0 (0.09)	42
RGD polystyrene				
Baseline	0.02 (0.05)	1.142 (0.002)	1.1 (0.03)	428
Histamine	0.03 (0.10)	1.125 (0.004)	1.1 (0.05)	143
Cyt-D	0.01 (0.10)	1.167 (0.004)	0.8 (0.05)	87

Values for stiffness (*A*) and viscosity (μ) are geometric means, with geometric SE in parentheses; values for slope (*x*) are means, with SE in parentheses. *N*, no. of beads. Values were measured at baseline or after exposure to histamine (10^{-4} M, 15 min) or cytochalasin D (Cyt-D; 2×10^{-6} M, 15 min) using beads coated with RGD (Arg-Gly-Asp), vitronectin (VN), urokinase plasminogen activator (uPA), acetylated low-density lipoprotein (AcLDL), several anti-β_1-integrin antibodies, and anti-β_3-integrin ($\alpha_v\beta_3$) antibody, as well as RGD-coated polystyrene beads.

Differences in stiffness from the largest values (Fig. 2*A*) to the smallest (Fig. 3*D*) approached two orders of magnitude. Despite these remarkable differences in magnitude, g′ and g″ in every case followed the same kind of weak power law behavior described by *Eq. 1* ($r^2 > 0.99$; solid lines in Figs. 2 and 3). Moreover, power law responses persisted on a cell-by-cell and bead-by-bead basis, and the power law exponent showed only modest bead-to-bead variability within each experimental condition (Table 1; Refs. 19, 20).

Existence and locus of the fixed point. For each bead coating we expressed the behavior over the bead population as the geometric mean of the scale factor *A* (*Eq. 1*), and the bead-by-bead variability as the geometric standard error (Table 1). We then assessed the existence of a common intersection, or fixed point. In the case of most bead coatings, constraint of the model (*Eq. 1*) to have a fixed point, implying common values of g_0, Φ_0 (*model II*) was not significantly different from allowing all parameters to be independent (*model I*) (see results in Table 3). Therefore, we adopted *model II* for these cases.

The exceptions were VN and activating antibody against β_1-integrin. In these cases *model I* fit the data significantly better than in *model II*. We adopted *model II* (the common fixed point) for these coatings as well, because that model fit the data extremely well ($r^2 > 0.990$; Table 2) and did so with one less parameter than *model I*. The case of uPA differed from the others in that these data were fit best by *model III* (Table 3). This result implies a parallel shift of the responses or, equivalently, that the common intersection, if it exists, is at such a high frequency that the lines are indistinguishable from being parallel within the range of measured frequencies.

The 95% confidence intervals for estimates of g_0 and Φ_0 showed a range of g_0 that, depending on bead type and bead coating, spanned two orders of magnitude. Confidence intervals for estimates of Φ_0 were very wide but overlapping (Fig. 4, Table 4). In the cases of uPA and anti-$\alpha_v\beta_3$-integrin coatings, the estimation of the intersection was very poor, with confidence intervals that were too large to make the identification of a fixed point (g_0, Φ_0) meaningful.

Scaling the data. Because power law responses were observed in every case, each of the fits (g′ vs. *f*) depicted in Figs. 2 and 3 can be defined by one point and one slope. The point was arbitrarily chosen as the value of g′ measured at 0.75 Hz, and the slope is $x - 1$. All relationships implied by the stiffness data in Figs. 2 and 3 could be represented compactly, therefore, by a graph of g′ (0.75 Hz) vs. *x* (Fig. 5).

When data were viewed in this way, several systematic trends became evident. First, within each of the coatings used, g′ and *x* changed in opposite directions among the three experimental conditions: histamine always yielded the highest values of stiffness and the lowest values of *x*, cytochalasin D always yielded the smallest values of stiffness and the highest values of *x*, and the baseline condition was always intermediate

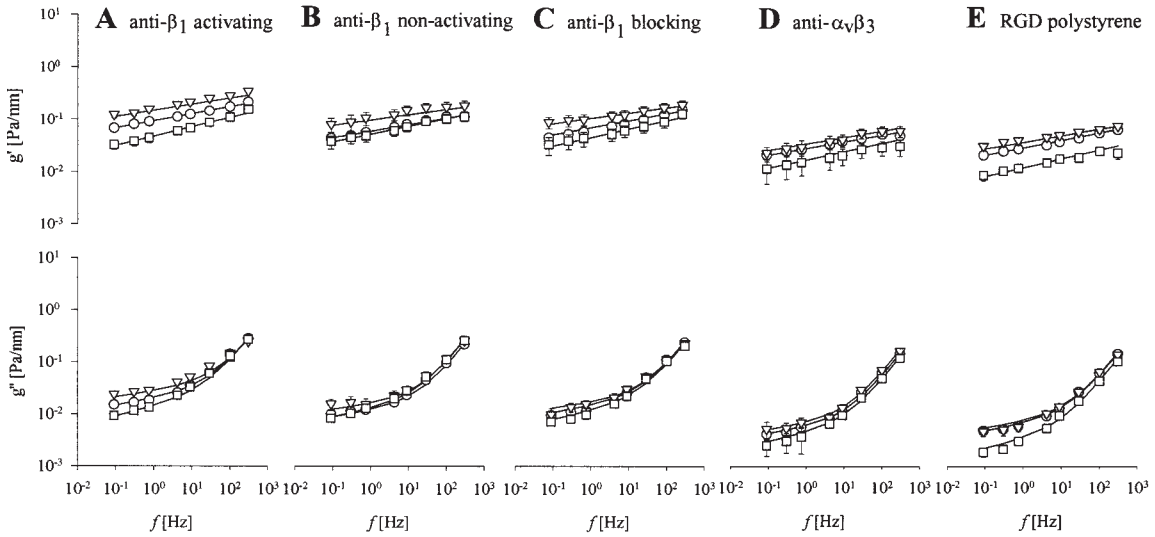

Fig. 3. Median values for g′ (*top*) and g′′ (*bottom*) vs. *f* for polystyrene beads antibody coated with activating anti-β_1-integrin (*A*), nonactivating anti-β_1-integrin (*B*), blocking anti-β_1-integrin (*C*), anti-β_3-integrin ($\alpha_v\beta_3$) (*D*), and RGD-coated polystyrene beads (*E*) in baseline conditions (○), histamine (10^{-4} M, 15 min; ▽), and cytochalasin D (2×10^{-6} M, 15 min; □). Solid lines are fits of *Eq. 1* to median data, and error bars represent 1 SE.

(Fig. 5). Second, across bead coatings (for the same experimental condition), the opposite trend was observed: as *x* increased, stiffness did as well. Moreover, differences in the measured stiffness approached two orders of magnitude. For g″ data, similar trends and differences were apparent (data not shown). Finally, the effect of the treatments on g′ and *x* varied widely depending on the bead coating: for example, after histamine treatment, stiffness increased 1.9-fold for beads coated with RGD but not at all for beads coated with anti-$\alpha_v\beta_3$-integrin.

For all bead coatings in which a fixed point could be determined (i.e., all but uPA and anti-$\alpha_v\beta_3$-integrins; Table 4), we used g_0 as an intrinsic stiffness scale and then defined a normalized stiffness G as the ratio of g′ measured at 0.75 Hz to g_0. When stiffness data in Fig. 5 were normalized in this way, they collapsed onto a single master relationship (Fig. 6*A*). We scaled the loss modulus g″ (0.75 Hz) by expressing it as a fraction of g′ at the same frequency; the ratio is $\eta = g''/g'$, known as the loss tangent or the hysteresivity. Similarly, despite enormous differences in g″ between experimental conditions, coating ligands, and bead type, all data collapsed onto a single relationship without exception (Fig. 6*B*). Some systematic discrepancies were noted, however, at larger values of *x*, where η varied with *x* in a way that was stronger than predicted.

DISCUSSION

As expected, the magnitude and the frequency dependence of elastic and loss moduli differed widely according to the experimental intervention, the type of bead, and the bead coating. Nonetheless, in every instance data conformed to a weak power law dependence of cell stiffness and friction upon frequency, according to *Eq. 1*. With few exceptions, cell stiffness data could be scaled onto a unifying relationship. With no exceptions, friction data could be described by a single unifying relationship. Accordingly, responses measured using different bead types and different bead coatings corresponded to different regions of the same master relationships in which *x* was seen to represent a central controlling parameter.

There are severe limitations inherent in the magnetic microbead approach. However, these limitations are counterbalanced in many applications by its unique capabilities. We begin by addressing those limitations and then move on to

Table 2. *Statistical evaluation of fit of the power law behavior (Eq. 1) to median data for models I, II, and III*

	Model I			*Model II*			*Model III*		
	r^2	r_{ss}, Pa^2/nm^2	df	r^2	r_{ss}, Pa^2/nm^2	df	r^2	r_{ss}, Pa^2/nm^2	df
RGD	0.994	0.159	45	0.994	0.159	46	0.987	0.373	47
VN	0.994	0.123	45	0.993	0.148	46	0.988	0.269	47
uPA	0.995	0.102	45	0.994	0.110	46	0.994	0.116	47
AcLDL	0.990	0.146	45	0.989	0.157	46	0.987	0.194	47
Anti-β_1 activating	0.995	0.051	39	0.994	0.068	40	0.987	0.145	41
Anti-β_1 nonactivating	0.995	0.047	39	0.994	0.051	40	0.987	0.113	41
Anti-β_1 blocking	0.991	0.085	39	0.991	0.087	40	0.982	0.166	41
Anti-$\alpha_v\beta_3$	0.995	0.066	39	0.995	0.068	40	0.995	0.073	41
RGD polystyrene	0.995	0.077	39	0.994	0.083	40	0.992	0.123	41

Median data are presented as correlation coefficients (r^2), residual variances (r_{ss}), and degrees of freedom (df) for each model.

Table 3. *Pairwise P-statistic comparisons of model II vs. model I and model III vs. model I by ANOVA F-test for reduction of variance*

	Model II vs. *Model I*	*Model III* vs. *Model I*
RGD	0.93	<0.01
VN	<0.01	<0.01
uPA	0.07	0.06
AcLDL	0.07	<0.01
Anti-β_1 activating	<0.01	<0.01
Anti-β_1 nonactivating	0.07	<0.01
Anti-β_1 blocking	0.38	<0.01
Anti-$\alpha_v\beta_3$	0.24	<0.01
RGD polystyrene	0.08	<0.01

For *model II* vs. *model I*, values of $P > 0.05$ imply that *model II* fits the data as well as *model I* and, therefore, that the data are consistent with the existence of a fixed point. For *model III* vs. *model I*, values of $P > 0.05$ imply that *model III* fits the data as well as *model I*, implying a parallel shift.

Table 4. *Estimated parameter values for g_0 and Φ_0 for model II, with median data*

	g_0, Pa/nm	Φ_0, rad/s
RGD	44.92 (1.60)	4.09×10^{10} (10.44)
VN	5.63 (1.68)	8.36×10^{9} (16.96)
uPA		
AcLDL	0.89 (1.99)	3.22×10^{10} (309.69)
Anti-β_1 activating	2.39 (1.51)	3.34×10^{10} (15.81)
Anti-β_1 nonactivating	0.51 (1.27)	9.79×10^{7} (7.11)
Anti-β_1 blocking	0.46 (1.31)	2.57×10^{7} (7.78)
Anti-$\alpha_v\beta_3$		
RGD polystyrene	0.92 (2.07)	9.67×10^{12} (249.22)

Values are estimated, from median data, for coordinates (g_0, Φ_0) of a fixed point. Geometric SD of the estimates are shown in parentheses. Estimations were very poor for uPA and anti-$\alpha_v\beta_3$-integrin coatings, with confidence intervals so large that identification of a fixed point was not meaningful.

address power law behavior, the marked differences in responses that are revealed when various molecular bead coatings are used, and finally, the commonality of those responses that are revealed when data are appropriately normalized.

Methodological limitations. Whether by ligation and/or mechanotransduction, the interaction of the magnetic microbead with the cell induces local remodeling events that alter the structure that is being probed (11, 14, 18, 22, 33, 59, 75). This remodeling is the principal weakness of the microbead approach but, at the same time, is one of its greatest strengths. While the bead has caused the cell to remodel locally (see Figs. 1 and 7), these remodeled structures are no different in kind from those that form at anchorage sites to the extracellular matrix (ECM) upon which the cell is adherent; indeed, from the point of view of the adherent cell, the bead is merely another piece of ECM upon which adhesion sites might be generated (11, 62, 74, 84). Because force transmission across the cell membrane occurs preferentially through adhesion molecules, and the adhesion complex in particular (4, 29, 42, 43, 62, 74, 84, 90), from the point of view of physiological relevance these would seem to be the most appropriate molecular pathways through which to probe cell mechanics. Probing the cell through a ligand-coated or antibody-coated bead offers the further advantage, therefore, of a defined molecular coupling rather than a nonspecific coupling. For these reasons, bead binding and mechanical loading have become standard tools for probing cell mechanics in the arsenal of approaches that are used for the investigation of adhesion site formation, mechanotransduction, and reinforcement (10, 12, 32, 33, 46, 86).

Other weaknesses of the magnetic microbead probe are that the position at which the bead settles onto the cell surface cannot be controlled (although it can be measured) and that the geometry of the bead-cell interaction also is not controlled (although, again, it can be measured) (4, 53). As with all probes of cell mechanics, the resulting state of stress within the cell is complicated (40, 60); in particular, Hu et al. (40) showed that stresses applied through RGD-coated microbeads are focused and transmitted at great lengths through the cell body via stress fibers.

A principal strength of the approach is that the bead can apply a mechanical load to the cell body in the physiological range of stress, from below 1 Pa to >100 Pa (20, 56). These loads are transmitted to the cell body via specific receptor-ligand systems, and the resulting bead displacements can be resolved on the molecular scale [as small as 5 nm (19, 20)]. Dynamic responses can be measured at frequencies as high as 1 kHz (19). Even at the highest frequencies studied, inertia does not come into play, and the effects of viscous loads associated with the medium are smaller than the loads associated with the cell by several orders of magnitude (20). Also, artifacts associated with the local heating caused by laser traps are not an issue.

Mechanical properties of cells in culture are innately variable from cell to cell. Detecting differences of 25% using an unpaired, one-tailed *t*-test requires roughly 50 cells per group, and detecting differences of 25% in baseline stiffness requires

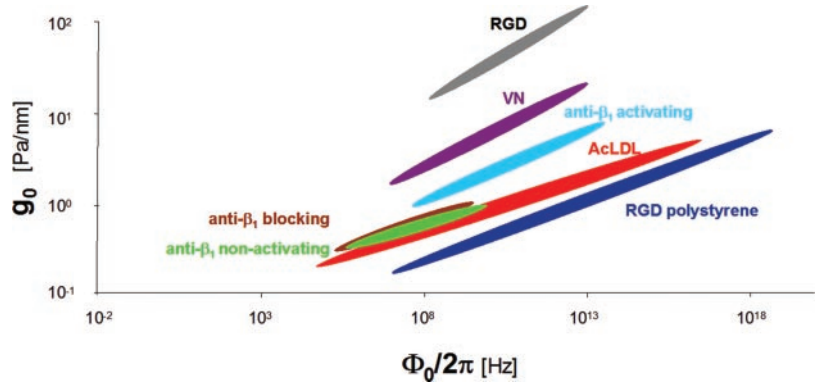

Fig. 4. The 95% confidence intervals are shown for the common fixed point (g_0, Φ_0) for (*top* to *bottom*) RGD (gray), VN (purple), activating anti-β_1-integrin (light blue), AcLDL (red), RGD polystyrene (dark blue), blocking anti-β_1-integrin (brown), and nonactivating anti-$\alpha_v\beta_3$-integrin (green) bead coatings.

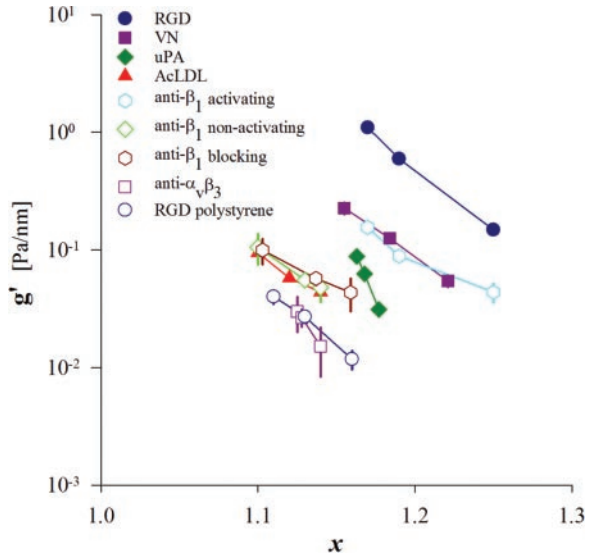

Fig. 5. Median values for g′ (0.75 Hz) vs. median values for slope factor *x* for RGD, VN, uPA, AcLDL, activating anti-β_1-integrin, nonactivating anti-β_1-integrin, blocking anti-β_1-integrin, anti-$\alpha_v\beta_3$-integrin, and RGD polystyrene bead coatings. Error bars represent 1 SE.

roughly 75 cells per group (21). The requirement of relatively large sample sizes is problematic for techniques that study one cell at a time, such as the use of atomic force microscopy or laser tweezers. Many beads can be tracked simultaneously by using magnetic twisting cytometry (MTC) with optical detection, by contrast, and data from hundreds or even thousands of cells can be collected within a relatively short time (20, 21).

Importantly, cells probed with this technology display mechanical responsiveness that is consistent with physiological responses measured at the tissue and organ levels. Panettieri et al. (67) showed that nontransformed HASM cells that are serum deprived and grown to confluence retain smooth muscle-specific contractile protein expression (α-actin and desmin), though not as much as freshly dissociated cells. These cells retain physiological responsiveness, including cytosolic Ca^{2+} release and cAMP production, in response to histamine, leukotrienes, bradykinin, platelet-activating factor, substance P, and thromboxane analogs (21, 41, 49, 67, 78). Using MTC, Hubmayr et al. (41) showed that cultured HASM cells stiffen when challenged with a panel of contractile agonists reported to increase intracellular Ca^{2+} concentration or inositol 1,4,5-trisphosphate formation and that the extent of cell stiffening rank is in order with the relative potency of these same agonists in mediating bronchoconstriction at the level of isolated muscle strips (24–26, 35). Conversely, cell stiffness decreases progressively with increasing doses of bronchodilating agonists that are known to increase intracellular cAMP and cGMP levels (41, 78). Shore and colleagues (41, 64, 78) showed that these cells retain functional coupling to β-adrenergic receptors over many population doublings. An et al. (3) found that serotonin (5-HT) increases cell stiffness in a dose-dependent fashion and also elicits rapid formation of F-actin, whereas a calmodulin antagonist, a myosin light chain kinase inhibitor, and a myosin ATPase inhibitor each ablate the stiffening response but not the F-actin polymerization induced by 5-HT. However, agents that inhibit the formation of F-actin attenuate both baseline stiffness and the extent of cell stiffening in response to 5-HT (3).

As with many of the available methods for measurement of cell mechanics (1, 6, 7, 12, 17, 38, 39, 72, 93), a length scale α, described in MATERIALS AND METHODS, must be invoked to convert raw data into a proper elastic modulus. Such a length scale can be computed using a finite element model of cell deformation (60) or estimated from simple dimensional arguments. In many instances, however, dynamic data either can be expressed as relative changes or can be nondimensionalized in such a way that this length scale cancels out (Fig. 6) and, therefore, does not come into play. Below we deal in more

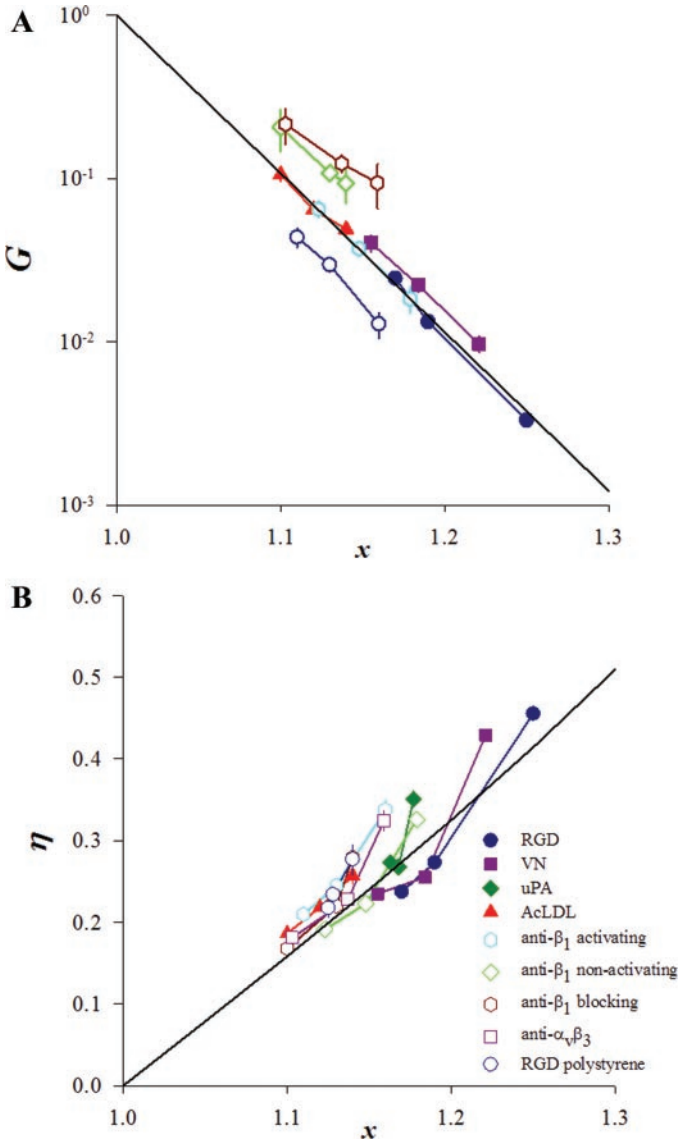

Fig. 6. Master curves for normalized stiffness G = g′ (0.75 Hz)/g_0 (*A*) and hysteresivity η (0.75 Hz) (*B*) vs. *x* from *model II* for RGD, VN, uPA, AcLDL, activating anti-β_1-integrin, nonactivating anti-β_1-integrin, blocking anti-β_1-integrin, anti-$\alpha_v\beta_3$-integrin, and RGD polystyrene bead coatings. Solid lines are predictions from *Eq. 1*: $(\omega/\Phi_0)^{x-1}\Gamma(2-x)\cos[(x-1)\pi/2]$, with $\Phi_0/2\pi = 10^8$ rad/s and $\omega = 0.75$ Hz (*A*), and $\eta = \tan[(x-1)\pi/2]$ (*B*). The limit $x = 1$ corresponds to a perfect Hookean elastic solid, and the limit $x = 2$ corresponds to a perfect Newtonian viscous fluid. As such, observed values of *x* demonstrate a spectrum of cytoskeletal behaviors ranging between solid and fluid, with cells being found closer to the solid range of the spectrum.

detail with the microbead approach, implications of differences in bead coating, and the way that these data can be scaled.

Power law behavior. Power law behavior according to *Eq. 1* pertained over a wide range of circumstances without exception (Figs. 2 and 3). Moreover, power law behavior persisted on a cell-by-cell and bead-by-bead basis, and the power law exponent showed only modest variability within each experimental condition (Table 1; Refs. 19, 20). These observations rule out artifacts in which a multiplicity of relaxation time scales might be attributable to population averages that pool together data sampled from many different individual cells and from very different regions on each cell. In addition, power law responses are also observed when the cell is probed using atomic force microscopy (1), parallel-plate extension of single cells (79), optical tweezers (5, 15), or laser tracking microrheology (91). Taken together, these observations strongly support the conclusion that power law behavior is an intensive property of the cellular material that is being probed.

It might be argued in this connection that, rather than a power law, these data could be fit equally well by using a viscoelastic model comprising roughly two relaxation time scales per frequency decade, or eight in all for the frequency range reported in the present study. While this is true, such an interpretation requires assignment of an ad hoc distribution of time constants and represents nothing more than a different parameterization of the data, albeit one requiring eight free parameters instead of one.

The great value of using a mechanical assay to probe protein-protein dynamics is that the elastic modulus gives a direct indication of the number of molecular interactions, and the loss modulus (expressed as the hysteresivity, or loss tangent, η) gives a direct indication of their rate of turnover (19, 26, 37). Using that strategy, Fabry et al. (20) had set out initially to identify a small number of distinct internal time scales, molecular relaxation times, or time constants that might typify mechanical responses of the integrated cytoskeletal matrix. However, the power law responses that they found precluded that possibility, suggesting instead the existence of a great many relaxation processes contributing when the frequency of the imposed forcing is small, but very few as the frequency of the forcing is increased and slower processes become progressively frozen out of the response. Therefore, with regard to protein-protein interactions within the complex microenvironment of the intact living cytoskeleton, there is no internal time scale that can typify the dynamics. Instead, all time scales are present simultaneously but distributed very unevenly; the dynamics are scale free (89). Scale-free behavior is thus found to pertain not only at the level of topology of the protein-protein signaling network (45), the level of protein structure (48), and the level of the spatial distribution of individual proteins (23) but also at the level of dynamics of the protein-protein interactions (20).

In a network in which the formation of new bonds and the breaking of old ones are thermally driven, relaxation processes are characterized by exponential decay. The cytoskeletal matrix of the living cell, by contrast, tends to relax with functions that decay much more slowly, as do other nonequilibrium condensed systems (13, 20, 92). If scale-free responses prevail, then interpretations based on processes characterized by one or even several molecular relaxation time scales must be ruled out (6, 7, 47, 91, 93). Instead, Fabry and colleagues (18–20, 34) associated the exponent x with an effective temperature of the cytoskeletal matrix as described in the theory of soft glassy rheology of Sollich (80, 81).

Probe specificity. What then might account for the differences in measured values of g' and g'' associated with the various probes that were employed? As noted above, the binding of a bead to the cell via any particular ligand-receptor complex inevitably leads to a cascade of signaling events and structural remodeling in the vicinity of the bead. RGD-coated beads, for example, are known to bind to integrins (mostly but not exclusively to $\alpha_v\beta_1$), which cluster and recruit other proteins into adhesion complexes (12, 33, 52, 62, 63, 70, 77, 84). These complexes are tightly coupled to deeper cytoskeletal structures such as the stress fibers and the contractile machinery of the cell (3, 19, 33, 40, 41, 50, 58, 76).

Among the bead coatings studied, stiffness values measured through beads coated with RGD showed the biggest changes with CSK manipulations, contractile activation, and deactivation (Figs. 2 and 3; Refs. 21, 41, 50, 78, 88) and showed stiffness values 10-fold greater than those seen through beads coated with AcLDL. These observations and others (2, 51, 69) suggest that measurements using RGD-coated beads tend to emphasize mechanical properties of the deep cytoskeletal structures such as stress fibers and the cell's contractile machinery (Fig. 7). Particularly relevant in that regard are recent data showing cytoskeletal remodeling induced by the presence of a RGD-coated bead (14). Supporting this interpretation

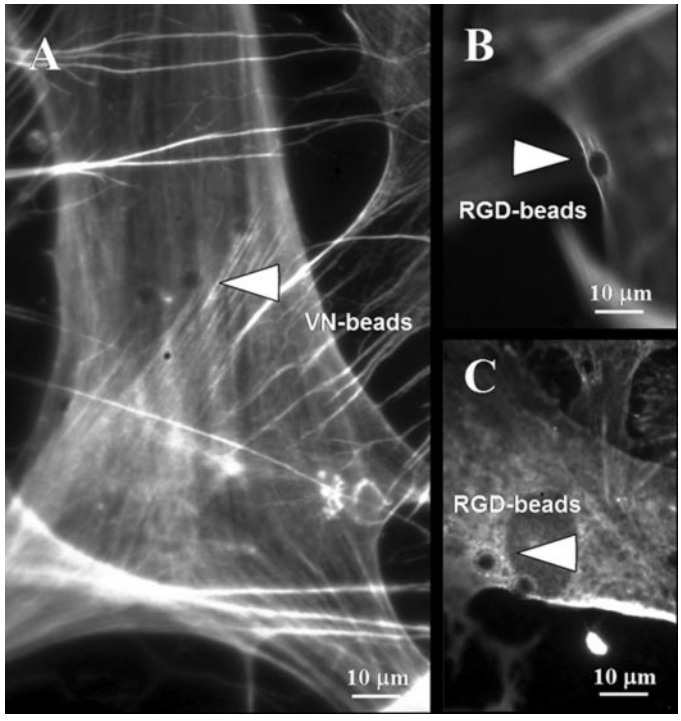

Fig. 7. Immunofluorescence images of HASM cells stained for F-actin. Arrowheads indicate increased density of F-actin in the vicinity of VN-coated (*A*) and RGD-coated beads (*B*). *C*: HASM cell stained for vinculin, a marker for adhesion complexes (30). Arrowhead indicates increased density of vinculin in the vicinity of an RGD-coated bead. For beads coated with uPA and activating antibodies, the F-actin staining on the bead site appeared less pronounced than for the rest of the coatings, including AcLDL (data not shown). Except for RGD-coated beads, vinculin had a diffuse staining pattern almost indistinguishable from the background.

further, Hu et al. (40) showed in the living adherent cell that stresses applied at the apical surface are transmitted via stress fibers over very long distances.

Beads coated with AcLDL bind to scavenger receptors, do not induce the formation of adhesion complexes, and are mechanically connected to stress fibers only indirectly if at all (11, 36, 70, 84, 85). As such, we speculate that they tend to emphasize the mechanics of the structures to which they are connected, which, in this case, would be cortical structures. If so, then the stiffness is likely to depend on lipid bilayer in-plane tension, membrane-CSK adhesions, and the strength of the link between the bead and those structures (73). This interpretation would help to explain the relatively smaller stiffness observed through AcLDL-coated beads as well as the attenuated effect of the CSK manipulations (Figs. 2–6). This result is also consistent with studies on the plasma membrane by Raucher and colleagues (29, 73).

In contrast with the behavior of beads (solid Fe_3O_4) coated with RGD, those coated with AcLDL reflect a value of x that is substantially smaller (1.118 ± 0.002 vs. 1.181 ± 0.002, at baseline). Similarly, beads coated with nonactivating and blocking anti-β_1-integrin antibodies, which do not promote the adhesion complexes formation and, hence, are only loosely connected to the deep CSK, also show relatively smaller values of x. Recalling that x is an index along the spectrum from solidlike ($x = 1$) to fluidlike ($x = 2$) states (*Eq. 1*), these observations suggest the interpretation that cortical structures are floppy but solidlike in character nonetheless, like a flimsy but stable elastic membrane, whereas stress fibers are closer to a fluidlike state.

For reasons that are unclear, RGD coatings on the two different bead types yielded very different mechanical responses (Fig. 5), with median stiffness values being different by more than one decade. Beads coated with activating anti-β_1-integrin were intermediate in that regard. Plausible explanations of these discrepancies might be differences in the amount of binding of peptide or antibody to the bead surface, differences in the availability of the molecular binding site to the receptor, or differences in geometrical arrangement of the binding site on the bead. These factors, in turn, would influence the extent to which the bead becomes embedded in the cell and the subcellular microenvironment that bead is probing (47, 57).

Scaled data. Despite the marked differences that were apparent in Figs. 2, 3 and 5, these diverse responses collapsed onto the same master curves (Fig. 6). As mentioned before, the values of the internal stiffness scale g_0 varied substantially among coatings, a result that was not unexpected. Confidence intervals for Φ_0 were extremely wide as a result of the combination of appreciable variability together with the small exponents of the power laws (Fig. 4). Nonetheless, Φ_0 could be set roughly in the neighborhood of 10^{10} Hz and, because of the wide confidence interval, could be taken as the same for all bead coatings.

The collapse of data imply that differences between RGD and AcLDL represent the extremes along a continuous spectrum of possibilities; the different bead types and various bead coatings that were studied always fell within the same class of responses (power law behavior) but with different power law exponents. In particular, the choice of the bead and its coating set the stiffness scale g_0, but once that stiffness scale was set, responses merely sampled different regions of the very same master curve (Fig. 6). Accordingly, except for the scale factor of normalization (g_0), the dynamics of the system, as characterized by the dependencies of g' and g'' on frequency, were set by x alone (Fig. 6; *Eq. 1*).

Special cases were beads coated with uPA and anti-$\alpha_v\beta_3$. These coatings conformed to the universal scaling with regard to friction (Fig. 6*B*) but not stiffness. The departure of these cases from the others stems from the fact that the power law responses of g' with f were nearly parallel, thereby making determination of a fixed point (and the internal stiffness scale g_0) not meaningful. We do not understand why these two instances are different in that regard. More generally, the finding of a fixed point stands as a serendipitous observation with no known explanation. As such, the physical meanings of the fixed point and the associated frequency scale Φ_0 remain unclear.

Surprising generality of these results. Elastic and frictional moduli reported in this study in cells measured under different circumstances and probed through different molecular windows were closely similar in character to measurements in a totally different kind of system, namely, colloid suspensions close to a jamming transition (71). Prasad et al. (71) interpreted their result with a very simple physical picture. They suggested that colloidal particles aggregate to form a solid network interspersed with background fluid. They reasoned that both the solid network and the viscous fluid contribute independently to the measured moduli. Because the background fluid is purely viscous, they argued that it contributes only to the loss modulus g'' and yields an additive term that increases linearly with frequency; Fabry et al. (20) came to much to the same conclusion. The scaling suggested by Prasad et al. (71), however, was flawed by an unrecognized but strong covariance of their scaling axes (for a weakly frequency-dependent complex stiffness plus a viscous term, their scaling is essentially a plot of g' vs. g'). Nevertheless, we can find no reason to suggest that the physical picture they describe might not apply to cytoskeletal dynamics. Moreover, they argued that if this picture is correct, then the viscosity should be independent of the factors that determine the configuration of the network, and, consistent with that argument, they found that the measured viscous term remained roughly independent of the network. Like theirs, our viscosity data (Table 1) are roughly consistent with that argument.

In summary, the findings reported here extend and generalize the results of Fabry et al. (19, 20), showing that power law responses and the collapse of data onto unifying master relationships (Fig. 6) are not peculiar to the RGD probe. *Equation 1* describes cell rheology without exception, and accordingly, we suspect that power law behavior must be a signature of some generic feature of underlying protein-protein interactions (20). In most cases, data collapsed onto unifying master relationships, implying that x, an index from solidlike ($x = 1$) to fluidlike ($x = 2$) behavior, is the central parameter that sets cytoskeletal dynamics (Fig. 6). These master relationships demonstrated that when a cell modulates its mechanical properties, it does so along a special trajectory.

Moreover, frequency responses of elastic and frictional moduli measured in different circumstances, and probed through a variety of different molecular windows, are similar to those found in colloid systems close to a jamming transition. We have speculated elsewhere that the cytoskeleton, like

certain colloid suspensions and other soft media, may belong to the class of soft glassy systems (19, 20, 34, 80, 81). Recently, such soft materials have been related to the jamming concept (54, 71, 82). Dynamics of soft glassy materials are entirely determined by the parameter x, which is called an effective matrix temperature (19, 20, 80, 81). All of these systems have the disordered molecular state of fluid and, at the same time, the rigidity of a solid. If these ideas apply to cytoskeletal behavior, they would point to metastability of interactions and disorder of the matrix as being key features of underlying protein-protein dynamics.

GRANTS

This work was supported by National Institutes of Health Grants HL-33009, HL/AI-65960, and HL-59682.

REFERENCES

1. **Alcaraz J, Buscemi L, Grabulosa M, Trepat X, Fabry B, Farre R, and Navajas D.** Microrheology of human lung epithelial cells measured by atomic force microscopy. *Biophys J* 84: 2071–2079, 2003.
2. **Alenghat FJ, Fabry B, Tsai KY, Goldmann WH, and Ingber DE.** Analysis of cell mechanics in single vinculin-deficient cells using a magnetic tweezer. *Biochem Biophys Res Commun* 277: 93–99, 2000.
3. **An SS, Laudadio RE, Lai J, Rogers RA, and Fredberg JJ.** Stiffness changes in cultured airway smooth muscle cells. *Am J Physiol Cell Physiol* 283: C792–C801, 2002.
4. **Balaban NQ, Schwarz US, Riveline D, Goichberg P, Tzur G, Sabanay I, Mahalu D, Safran S, Bershadsky A, Addadi L, and Geiger B.** Force and focal adhesion assembly: a close relationship studied using elastic micropatterned substrates. *Nat Cell Biol* 3: 466–472, 2001.
5. **Balland M, Richert A, and Gallet F.** Microrheology of the actin cytoskeleton: response to oscillating forces exerted with optical tweezers (Abstract). *Eur Respir J* 22, *Suppl* 44: 314, 2003.
6. **Bausch AR, Moller W, and Sackmann E.** Measurement of local viscoelasticity and forces in living cells by magnetic tweezers. *Biophys J* 76: 573–579, 1999.
7. **Bausch AR, Ziemann F, Boulbitch AA, Jacobson K, and Sackmann E.** Local measurements of viscoelastic parameters of adherent cell surfaces by magnetic bead microrheometry. *Biophys J* 75: 2038–2049, 1998.
8. **Burridge K and Chrzanowska-Wodnicka M.** Focal adhesions, contractility, and signaling. *Annu Rev Cell Dev Biol* 12: 463–518, 1996.
9. **Chapman HA.** Plasminogen activators, integrins, and the coordinated regulation of cell adhesion and migration. *Curr Opin Cell Biol* 9: 714–724, 1997.
10. **Chen J, Fabry B, Schiffrin EL, and Wang N.** Twisting integrin receptors increases endothelin-1 gene expression in endothelial cells. *Am J Physiol Cell Physiol* 280: C1475–C1484, 2001.
11. **Chicurel ME, Singer RH, Meyer CJ, and Ingber DE.** Integrin binding and mechanical tension induce movement of mRNA and ribosomes to focal adhesions. *Nature* 392: 730–733, 1998.
12. **Choquet D, Felsenfeld DP, and Sheetz MP.** Extracellular matrix rigidity causes strengthening of integrin-cytoskeleton linkages. *Cell* 88: 39–48, 1997.
13. **Cipelletti L, Manley S, Ball RC, and Weitz DA.** Universal aging features in the restructuring of fractal colloidal gels. *Phys Rev Lett* 84: 2275–2278, 2000.
14. **Deng L, Fairbank NJ, Fabry B, Smith PG, and Maksym GN.** Localized mechanical stress induces time-dependent actin cytoskeletal remodeling and stiffening in cultured airway smooth muscle cells. *Am J Physiol Cell Physiol* 287: C440–C448, 2004.
15. **Desprat N, Simeon J, Richert A, and Asnacios A.** Creep experiments on isolated myoblast show soft glassy materials behavior (Abstract). *Eur Respir J* 22, *Suppl* 44: 309, 2003.
16. **Djordjevic VD, Jaric J, Fabry B, Fredberg JJ, and Stamenović D.** Fractional derivatives embody essential features of cell rheological behavior. *Ann Biomed Eng* 31: 692–699, 2003.
17. **Evans E and Yeung A.** Apparent viscosity and cortical tension of blood granulocytes determined by micropipet aspiration. *Biophys J* 56: 151–160, 1989.
18. **Fabry B and Fredberg JJ.** Remodeling of the airway smooth muscle cell: are we built of glass? *Respir Physiol Neurobiol* 137: 109–124, 2003.
19. **Fabry B, Maksym GN, Butler JP, Glogauer M, Navajas D, and Fredberg JJ.** Scaling the microrheology of living cells. *Phys Rev Lett* 87: 148102, 2001.
20. **Fabry B, Maksym GN, Butler JP, Glogauer M, Navajas D, Taback NA, Millet EJ, and Fredberg JJ.** Time scale and other invariants of integrative mechanical behavior in living cells. *Phys Rev E Stat Nonlin Soft Matter Phys* 68: 041914, 2003.
21. **Fabry B, Maksym GN, Shore SA, Moore PE, Panettieri RA Jr, Butler JP, and Fredberg JJ.** Selected contribution: time course and heterogeneity of contractile responses in cultured human airway smooth muscle cells. *J Appl Physiol* 91: 986–994, 2001.
22. **Felsenfeld DP, Choquet D, and Sheetz MP.** Ligand binding regulates the directed movement of β_1 integrins on fibroblasts. *Nature* 383: 438–440, 1996.
23. **Fields S.** Proteomics. Proteomics in genomeland. *Science* 291: 1221–1224, 2001.
24. **Fredberg JJ, Inouye D, Miller B, Nathan M, Jafari S, Raboudi SH, Butler JP, and Shore SA.** Airway smooth muscle, tidal stretches, and dynamically determined contractile states. *Am J Respir Crit Care Med* 156: 1752–1759, 1997.
25. **Fredberg JJ, Inouye DS, Mijailovich SM, and Butler JP.** Perturbed equilibrium of myosin binding in airway smooth muscle and its implications in bronchospasm. *Am J Respir Crit Care Med* 159: 959–967, 1999.
26. **Fredberg JJ, Jones KA, Nathan M, Raboudi S, Prakash YS, Shore SA, Butler JP, and Sieck GC.** Friction in airway smooth muscle: mechanism, latch, and implications in asthma. *J Appl Physiol* 81: 2703–2712, 1996.
27. **Fredberg JJ and Stamenovic D.** On the imperfect elasticity of lung tissue. *J Appl Physiol* 67: 2408–2419, 1989.
28. **Fung Y.** *Biomechanics: Mechanical Properties of Living Tissues.* New York: Springer, 1989.
29. **Galbraith CG and Sheetz MP.** Keratocytes pull with similar forces on their dorsal and ventral surfaces. *J Cell Biol* 147: 1313–1324, 1999.
30. **Galbraith CG, Yamada KM, and Sheetz MP.** The relationship between force and focal complex development. *J Cell Biol* 159: 695–705, 2002.
31. **Geiger B, Bershadsky A, Pankov R, and Yamada KM.** Transmembrane crosstalk between the extracellular matrix—cytoskeleton crosstalk. *Nat Rev Mol Cell Biol* 2: 793–805, 2001.
32. **Giannone G, Jiang G, Sutton DH, Critchley DR, and Sheetz MP.** Talin1 is critical for force-dependent reinforcement of initial integrin-cytoskeleton bonds but not tyrosine kinase activation. *J Cell Biol* 163: 409–419, 2003.
33. **Glogauer M, Arora P, Yao G, Sokholov I, Ferrier J, and McCulloch CA.** Calcium ions and tyrosine phosphorylation interact coordinately with actin to regulate cytoprotective responses to stretching. *J Cell Sci* 110: 11–21, 1997.
34. **Gunst SJ and Fredberg JJ.** The first three minutes: smooth muscle contraction, cytoskeletal events, and soft glasses. *J Appl Physiol* 95: 413–425, 2003.
35. **Gunst SJ, Stropp JQ, and Flavahan NA.** Interaction of contractile responses in canine tracheal smooth muscle. *J Appl Physiol* 63: 514–520, 1987.
36. **Herz J and Marschang P.** Coaxing the LDL receptor family into the fold. *Cell* 112: 289–292, 2003.
37. **Hill AV.** *Trails and Trials in Physiology. A Bibliography, 1909–1964; with Reviews of Certain Topics and Methods and a Reconnaissance for Further Research.* London: Edward Arnold, 1965.
38. **Hochmuth RM.** Measuring the mechanical properties of individual human blood cells. *J Biomech Eng* 115: 515–519, 1993.
39. **Hochmuth RM.** Micropipette aspiration of living cells. *J Biomech* 33: 15–22, 2000.
40. **Hu S, Chen J, Fabry B, Numaguchi Y, Gouldstone A, Ingber DE, Fredberg JJ, Butler JP, and Wang N.** Intracellular stress tomography reveals stress focusing and structural anisotropy in cytoskeleton of living cells. *Am J Physiol Cell Physiol* 285: C1082–C1090, 2003.
41. **Hubmayr RD, Shore SA, Fredberg JJ, Planus E, Panettieri RA Jr, Moller W, Heyder J, and Wang N.** Pharmacological activation changes stiffness of cultured human airway smooth muscle cells. *Am J Physiol Cell Physiol* 271: C1660–C1668, 1996.
42. **Ingber D.** Integrins as mechanochemical transducers. *Curr Opin Cell Biol* 3: 841–848, 1991.

43. **Ingber DE.** Integrins, tensegrity, and mechanotransduction. *Gravit Space Biol Bull* 10: 49–55, 1997.
44. **Ingber DE, Dike L, Hansen L, Karp S, Liley H, Maniotis A, McNamee H, Mooney D, Plopper G, Sims J, and Wang N.** Cellular tensegrity: exploring how mechanical changes in the cytoskeleton regulate cell growth, migration, and tissue pattern during morphogenesis. *Int Rev Cytol* 150: 173–224, 1994.
45. **Jeong H, Tombor B, Albert R, Oltvai ZN, and Barabasi AL.** The large-scale organization of metabolic networks. *Nature* 407: 651–654, 2000.
46. **Jiang G, Giannone G, Critchley DR, Fukumoto E, and Sheetz MP.** Two-piconewton slip bond between fibronectin and the cytoskeleton depends on talin. *Nature* 424: 334–337, 2003.
47. **Karcher H, Lammerding J, Huang H, Lee RT, Kamm RD, and Kaazempur-Mofrad MR.** A three-dimensional viscoelastic model for cell deformation with experimental verification. *Biophys J* 85: 3336–3349, 2003.
48. **Koonin EV, Wolf YI, and Karev GP.** The structure of the protein universe and genome evolution. *Nature* 420: 218–223, 2002.
49. **Laporte JC, Moore PE, Baraldo S, Jouvin MH, Church TL, Schwartzman IN, Panettieri RA Jr, Kinet JP, and Shore SA.** Direct effects of interleukin-13 on signaling pathways for physiological responses in cultured human airway smooth muscle cells. *Am J Respir Crit Care Med* 164: 141–148, 2001.
50. **Laporte JD, Moore PE, Panettieri RA, Moeller W, Heyder J, and Shore SA.** Prostanoids mediate IL-1β-induced β-adrenergic hyporesponsiveness in human airway smooth muscle cells. *Am J Physiol Lung Cell Mol Physiol* 275: L491–L501, 1998.
51. **Lau AW, Hoffman BD, Davies A, Crocker JC, and Lubensky TC.** Microrheology, stress fluctuations, and active behavior of living cells. *Phys Rev Lett* 91: 198101, 2003.
52. **Lauffenburger DA and Horwitz AF.** Cell migration: a physically integrated molecular process. *Cell* 84: 359–369, 1996.
53. **Laurent VM, Fodil R, Canadas P, Fereol S, Louis B, Planus E, and Isabey D.** Partitioning of cortical and deep cytoskeleton responses from transient magnetic bead twisting. *Ann Biomed Eng* 31: 1263–1278, 2003.
54. **Liu AJ and Nagel SR.** Jamming is not just cool any more. *Nature* 396: 21–22, 1998.
55. **Liu S, Calderwood DA, and Ginsberg MH.** Integrin cytoplasmic domain-binding proteins. *J Cell Sci* 113: 3563–3571, 2000.
56. **Maksym GN, Fabry B, Butler JP, Navajas D, Tschumperlin DJ, Laporte JD, and Fredberg JJ.** Mechanical properties of cultured human airway smooth muscle cells from 0.05 to 0.4 Hz. *J Appl Physiol* 89: 1619–1632, 2000.
57. **McGrath JL, Hartwig JH, and Kuo SC.** The mechanics of F-actin microenvironments depend on the chemistry of probing surfaces. *Biophys J* 79: 3258–3266, 2000.
58. **Mehta D and Gunst SJ.** Actin polymerization stimulated by contractile activation regulates force development in canine tracheal smooth muscle. *J Physiol* 519: 829–840, 1999.
59. **Meyer CJ, Alenghat FJ, Rim P, Fong JH, Fabry B, and Ingber DE.** Mechanical control of cyclic AMP signalling and gene transcription through integrins. *Nat Cell Biol* 2: 666–668, 2000.
60. **Mijailovich SM, Kojic M, Zivkovic M, Fabry B, and Fredberg JJ.** A finite element model of cell deformation during magnetic bead twisting. *J Appl Physiol* 93: 1429–1436, 2002.
61. **Miranti CK and Brugge JS.** Sensing the environment: a historical perspective on integrin signal transduction. *Nat Cell Biol* 4: E83–E90, 2002.
62. **Miyamoto S, Akiyama SK, and Yamada KM.** Synergistic roles for receptor occupancy and aggregation in integrin transmembrane function. *Science* 267: 883–885, 1995.
63. **Miyamoto S, Teramoto H, Coso OA, Gutkind JS, Burbelo PD, Akiyama SK, and Yamada KM.** Integrin function: molecular hierarchies of cytoskeletal and signaling molecules. *J Cell Biol* 131: 791–805, 1995.
64. **Moore PE, Laporte JD, Abraham JH, Schwartzman IN, Yandava CN, Silverman ES, Drazen JM, Wand MP, Panettieri RA Jr, and Shore SA.** Polymorphism of the β_2-adrenergic receptor gene and desensitization in human airway smooth muscle. *Am J Respir Crit Care Med* 162: 2117–2124, 2000.
65. **Mukhina S, Stepanova V, Traktouev D, Poliakov A, Beabealashvilly R, Gursky Y, Minashkin M, Shevelev A, and Tkachuk V.** The chemotactic action of urokinase on smooth muscle cells is dependent on its kringle domain. Characterization of interactions and contribution to chemotaxis. *J Biol Chem* 275: 16450–16458, 2000.
66. **Ossowski L and Aguirre-Ghiso JA.** Urokinase receptor and integrin partnership: coordination of signaling for cell adhesion, migration and growth. *Curr Opin Cell Biol* 12: 613–620, 2000.
67. **Panettieri RA, Murray RK, DePalo LR, Yadvish PA, and Kotlikoff MI.** A human airway smooth muscle cell line that retains physiological responsiveness. *Am J Physiol Cell Physiol* 256: C329–C335, 1989.
68. **Planus E, Barlovatz-Meimon G, Rogers RA, Bonavaud S, Ingber DE, and Wang N.** Binding of urokinase to plasminogen activator inhibitor type-1 mediates cell adhesion and spreading. *J Cell Sci* 110: 1091–1098, 1997.
69. **Plopper G and Ingber DE.** Rapid induction and isolation of focal adhesion complexes. *Biochem Biophys Res Commun* 193: 571–578, 1993.
70. **Plopper GE, McNamee HP, Dike LE, Bojanowski K, and Ingber DE.** Convergence of integrin and growth factor receptor signaling pathways within the focal adhesion complex. *Mol Biol Cell* 6: 1349–1365, 1995.
71. **Prasad V, Trappe V, Dinsmore AD, Segre PN, Cipelletti L, and Weitz DA.** Rideal lecture. Universal features of the fluid to solid transition for attractive colloidal particles. *Faraday Discuss* 123: 1–12; discussion 75–97, 419–421, 2003.
72. **Radmacher M, Fritz M, Kacher CM, Cleveland JP, and Hansma PK.** Measuring the viscoelastic properties of human platelets with the atomic force microscope. *Biophys J* 70: 556–567, 1996.
73. **Raucher D and Sheetz MP.** Membrane expansion increases endocytosis rate during mitosis. *J Cell Biol* 144: 497–506, 1999.
74. **Riveline D, Zamir E, Balaban NQ, Schwarz US, Ishizaki T, Narumiya S, Kam Z, Geiger B, and Bershadsky AD.** Focal contacts as mechanosensors: externally applied local mechanical force induces growth of focal contacts by an mDia1-dependent and ROCK-independent mechanism. *J Cell Biol* 153: 1175–1186, 2001.
75. **Schmidt C, Pommerenke H, Durr F, Nebe B, and Rychly J.** Mechanical stressing of integrin receptors induces enhanced tyrosine phosphorylation of cytoskeletally anchored proteins. *J Biol Chem* 273: 5081–5085, 1998.
76. **Schoenwaelder SM and Burridge K.** Bidirectional signaling between the cytoskeleton and integrins. *Curr Opin Cell Biol* 11: 274–286, 1999.
77. **Schwartz MA, Lechene C, and Ingber DE.** Insoluble fibronectin activates the Na/H antiporter by clustering and immobilizing integrin $\alpha_5\beta_1$, independent of cell shape. *Proc Natl Acad Sci USA* 88: 7849–7853, 1991.
78. **Shore SA, Laporte J, Hall IP, Hardy E, and Panettieri RA Jr.** Effect of IL-1β on responses of cultured human airway smooth muscle cells to bronchodilator agonists. *Am J Respir Cell Mol Biol* 16: 702–712, 1997.
79. **Smith PG, Deng L, Fredberg JJ, and Maksym GN.** Mechanical strain increases cell stiffness through cytoskeletal filament reorganization. *Am J Physiol Lung Cell Mol Physiol* 285: L456–L463, 2003.
80. **Sollich P.** Rheological constitutive equation for a model of soft glassy materials. *Phys Rev E* 58: 738–759, 1998.
81. **Sollich P, Lequeux F, Hébraud P, and Cates ME.** Rheology of soft glassy materials. *Phys Rev Lett* 78: 2020–2023, 1997.
82. **Trappe V, Prasad V, Cipelletti L, Segre PN, and Weitz DA.** Jamming phase diagram for attractive particles. *Nature* 411: 772–775, 2001.
83. **Tsuruta D, Gonzales M, Hopkinson SB, Otey C, Khuon S, Goldman RD, and Jones JC.** Microfilament-dependent movement of the β_3 integrin subunit within focal contacts of endothelial cells. *FASEB J* 16: 866–868, 2002.
84. **Wang N, Butler JP, and Ingber DE.** Mechanotransduction across the cell surface and through the cytoskeleton. *Science* 260: 1124–1127, 1993.
85. **Wang N and Ingber DE.** Control of cytoskeletal mechanics by extracellular matrix, cell shape, and mechanical tension. *Biophys J* 66: 2181–2189, 1994.
86. **Wang N and Ingber DE.** Probing transmembrane mechanical coupling and cytomechanics using magnetic twisting cytometry. *Biochem Cell Biol* 73: 327–335, 1995.
87. **Wang N, Planus E, Pouchelet M, Fredberg JJ, and Barlovatz-Meimon G.** Urokinase receptor mediates mechanical force transfer across the cell surface. *Am J Physiol Cell Physiol* 268: C1062–C1066, 1995.
88. **Wang N, Tolic-Norrelykke IM, Chen J, Mijailovich SM, Butler JP, Fredberg JJ, and Stamenović D.** Cell prestress. I. Stiffness and prestress are closely associated in adherent contractile cells. *Am J Physiol Cell Physiol* 282: C606–C616, 2002.
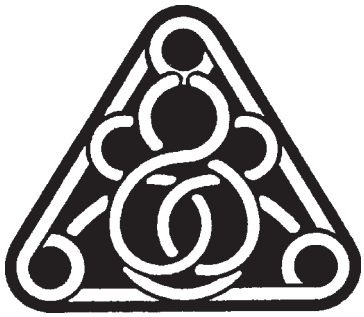
89. **Wilson TA.** Time constants may be meaningless in exponentials fit to pressure relaxation data. *J Appl Physiol* 77: 1570–1571, 1994.
90. **Yamada KM and Geiger B.** Molecular interactions in cell adhesion complexes. *Curr Opin Cell Biol* 9: 76–85, 1997.
91. **Yamada S, Wirtz D, and Kuo SC.** Mechanics of living cells measured by laser tracking microrheology. *Biophys J* 78: 1736–1747, 2000.
92. **Yang H, Luo G, Karnchanaphanurach P, Louie TM, Rech I, Cova S, Xun L, and Xie XS.** Protein conformational dynamics probed by single-molecule electron transfer. *Science* 302: 262–266, 2003.
93. **Ziemann F, Radler J, and Sackmann E.** Local measurements of viscoelastic moduli of entangled actin networks using an oscillating magnetic bead micro-rheometer. *Biophys J* 66: 2210–2216, 1994.